Supplementary Information:

Transcranial optogenetic brain modulator for precise bimodal neuromodulation in multiple brain regions

Shin et al.

`

	Proposed system	**[1]Li et al., 2022**	**[2]Kim et al., 2021**	**[3]Yang et al., 2021**
Invasive or non-invasive	**Non-invasive**	Invasive	Invasive	Invasive
Depth of stimulation	**~ 3 mm**	No limits	No limits	No limits
Multiple site modulation	**Yes**	No	Yes	Yes
Number of the sites	**4**	1	2	2
Bimodal modulation	**Yes**	Yes	No	No
LED's colors	**Red / NIR**	Blue / Red	Blue	Blue
Size (mm^2)	**19 x 12 mm^2**	22 x 13 mm^2	19 x 12 mm^2	10 x 12 mm^2
Weight (g)	**1.9 g (including 30 mAh LiPo battery)**	1.9 g (including 35 mAh Li-ion battery)	1.4 g (including 12 mAh LiPo battery)	< 1 g (wireless power transfer)

Supplementary Table 1: A summary of our device`s performance and comparison with previously developed wireless optoelectronic brain modulator.

	Resistance (Ω)	Temperature (°C)
Red, continuous operation, without the plastic-based thermal isolator	130.1	77.9
NIR, continuous operation, without the plastic-based thermal isolator	134.0	88.1
Red, 10 Hz, 10 ms (10% duty cycle), without the plastic-based thermal isolator	114.4	37.0
NIR, 10 Hz, 10 ms (10% duty cycle), without the plastic-based thermal isolator	115.2	39.1
Red, 10 Hz, 10 ms (10% duty cycle), with the plastic-based thermal isolator	113.4	34.5
NIR, 10 Hz, 10 ms (10% duty cycle), with the plastic-based thermal isolator	114.3	36.8

Supplementary Table 2: Thermal measurements of LED operation under various conditions. This table presents the resistance and corresponding temperature measurements for red and NIR LEDs under various operational conditions. The temperatures were calculated using the calculation formula provided by the provider.

$$R(T) = R(0) \times (1 + a \times T + b \times T^2)$$

where $R(T)$ is the resistance at temperature T,

$R(0)$ = 100Ω, which is the resistance at 0°C,

$a = 3.9083 \times 10^{-3}$,

$b = -5.775 \times 10^{-7}$.

The temperature measurement includes an error margin of $\pm\left(0.15 + 0.002 \times \left|\frac{T}{°C}\right|\right)°C$, reflecting the precision of the thermistor.

Distance between LED and paper ruler (mm)	Range of light spread on a paper ruler (mm)
1	2
2	3
3	4
4	5

Supplementary Table 3: Measurement of light spread from the LED. This table presents the measured range of light spread from the LED onto a paper ruler at varying distances.

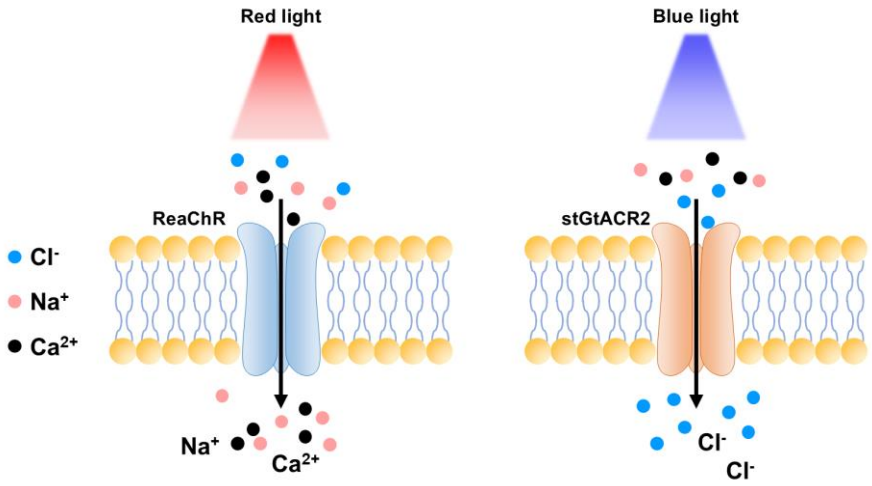

Supplementary Fig. 1: Schematic diagram of optogenetic modulation at the cellular scale. The process involves using light to regulate the activity of specific channels in cells. In this case, the cation channel ReaChR is depolarized by red light, while the anion channel stGtACR2 is hyperpolarized by blue light.

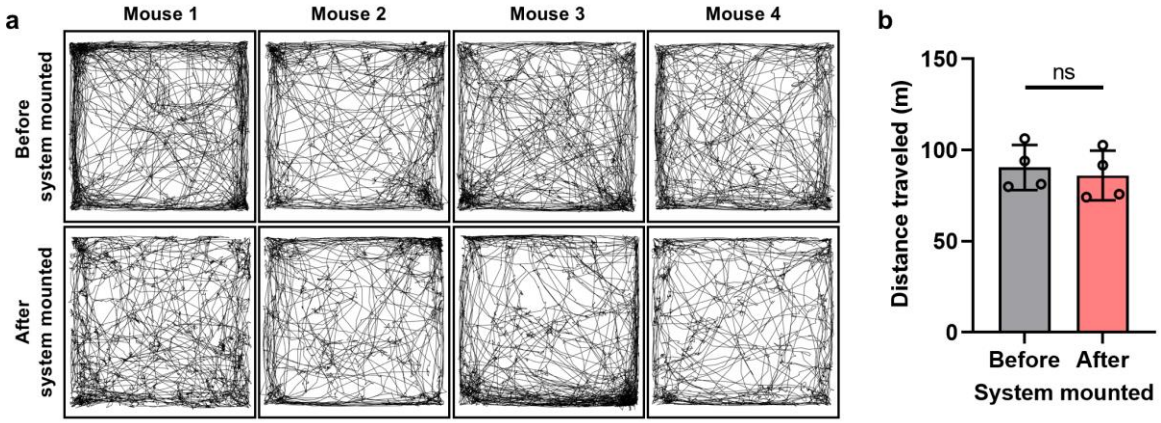

Supplementary Fig. 2: The effect of an optoelectronic system on general locomotor activity in mice. a Trajectories of each mouse before and after mounting the system for 30 min. **b** Comparison of the distance traveled by the mice before and after mounting the system on their heads (p=0.12500, white circle: n=4 where n is the number of mice.). The data are presented as mean values +/− s.d. with individual data points. Statistical analysis was performed by the two-tailed Mann-Whitney test, and $p<0.05$ was considered significant. ns: no statistical significance.

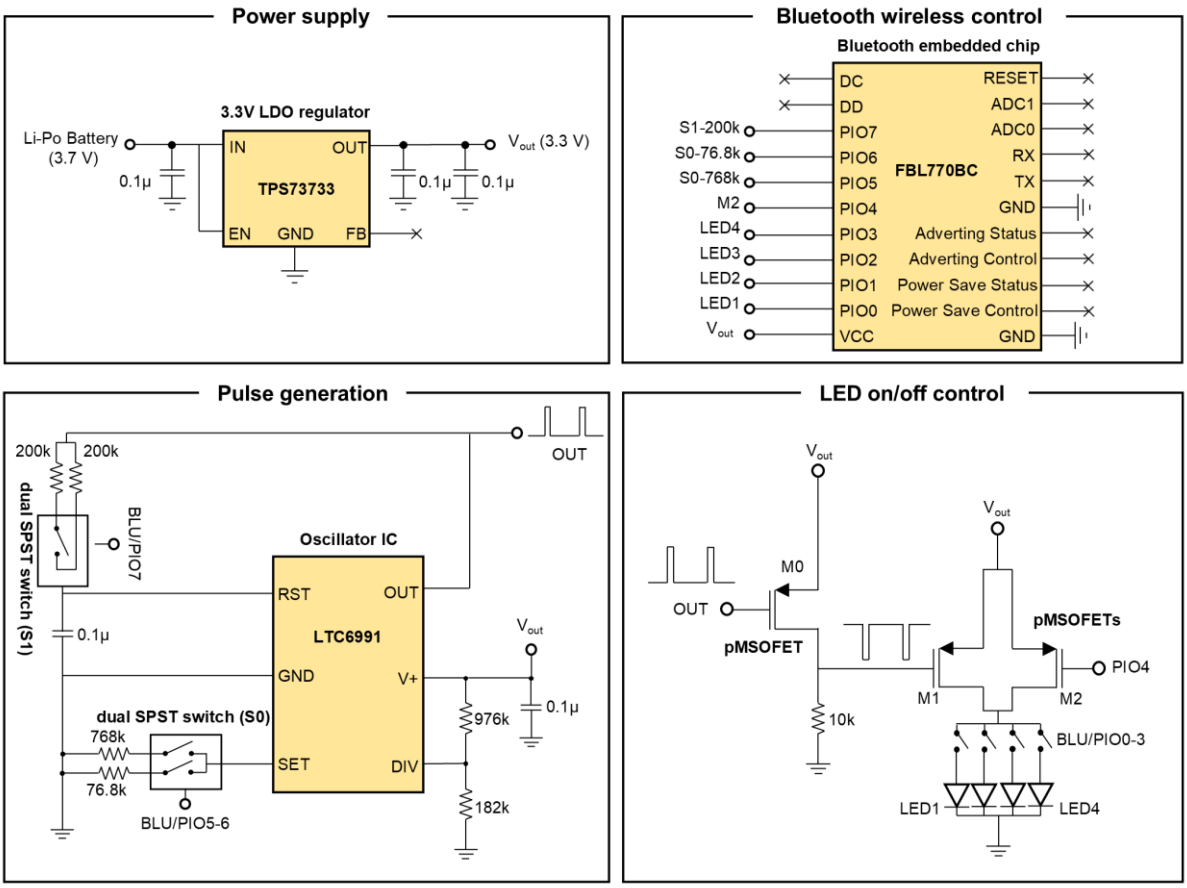

Supplementary Fig. 3: Circuit diagram for the wireless control module.

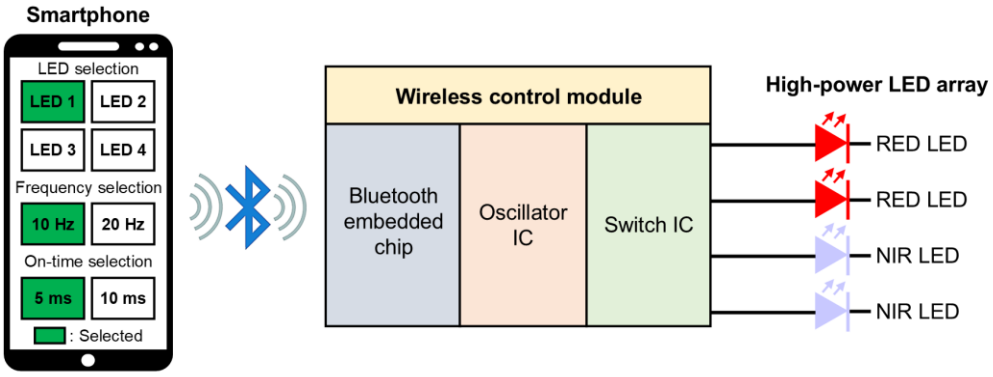

Supplementary Fig. 4: Schematic diagram that illustrates the operation of the wireless control module.

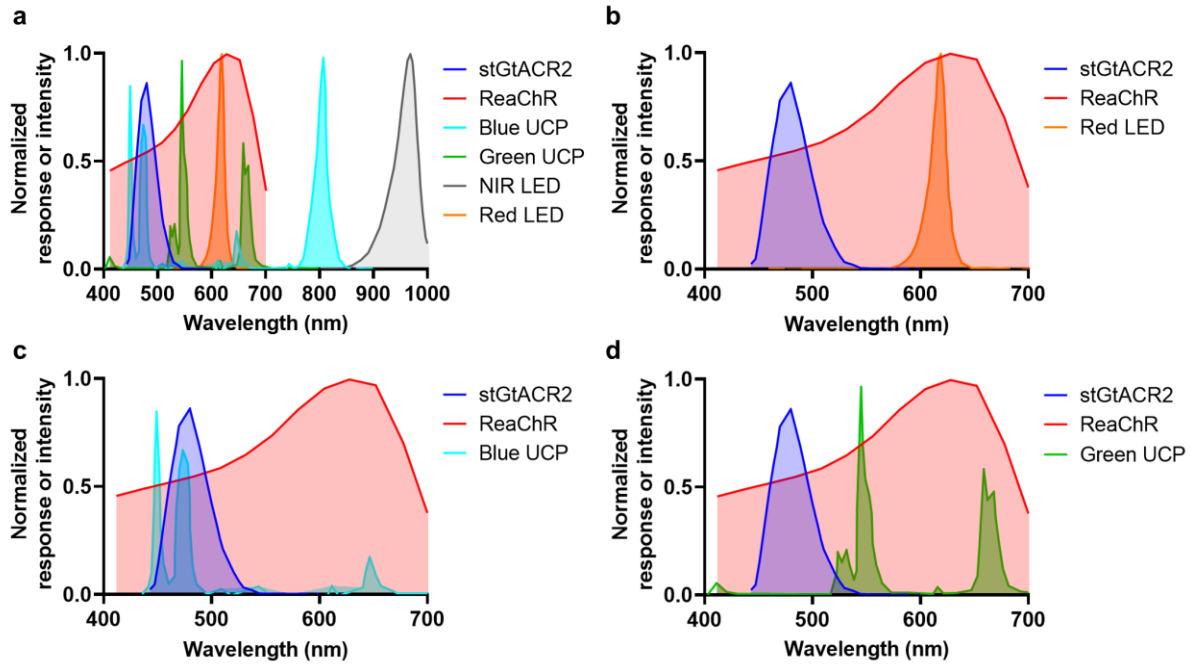

Supplementary Fig. 5: Spectral overlap of opsins and light sources. a Full spectral analysis. The normalized response or intensity spectra of stGtACR2, ReaChR, Blue UCP, Green UCP, NIR LED, and Red LED. **b** The spectral overlap between the Red LED, ReaChR, and stGtACR2. **c** The spectral overlap between the Blue UCP, ReaChR, and stGtACR2. **d** The spectral overlap between the Green UCP, ReaChR, and stGtACR2.

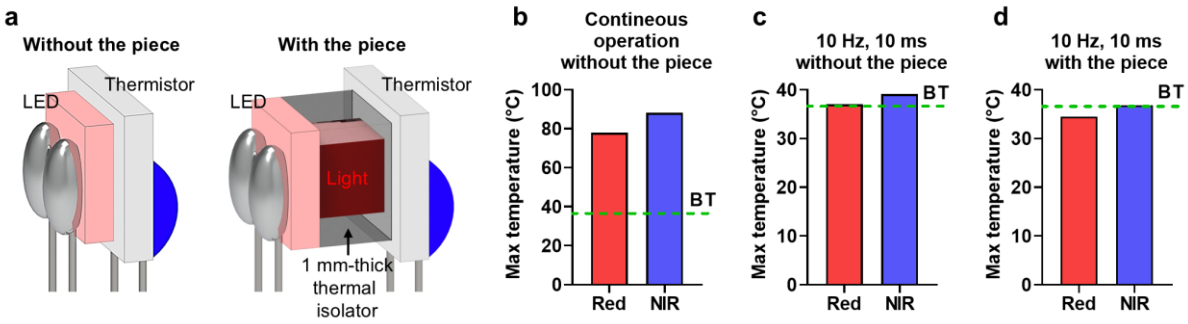

Supplementary Fig. 6: Thermal measurements of Red and NIR LEDs with and without a plastic-based thermal isolator. a Schematic of the thermal measurement setup. Illustrations showing the experimental setup used for measuring the temperature of LEDs, both with and without a 1 mm-thick thermal isolator of thermal isolator. A thermistor is attached to record temperature changes during LED operation. **b** Maximum temperature during continuous operation without the thermal isolator. **c** Maximum temperature at 10 Hz, 10 ms without the thermal isolator. **d** Maximum temperature at 10 Hz, 10 ms with the thermal isolator. In each graph, the dotted line labeled "BT" indicates the body temperature of a mouse, which is 36.6°C.

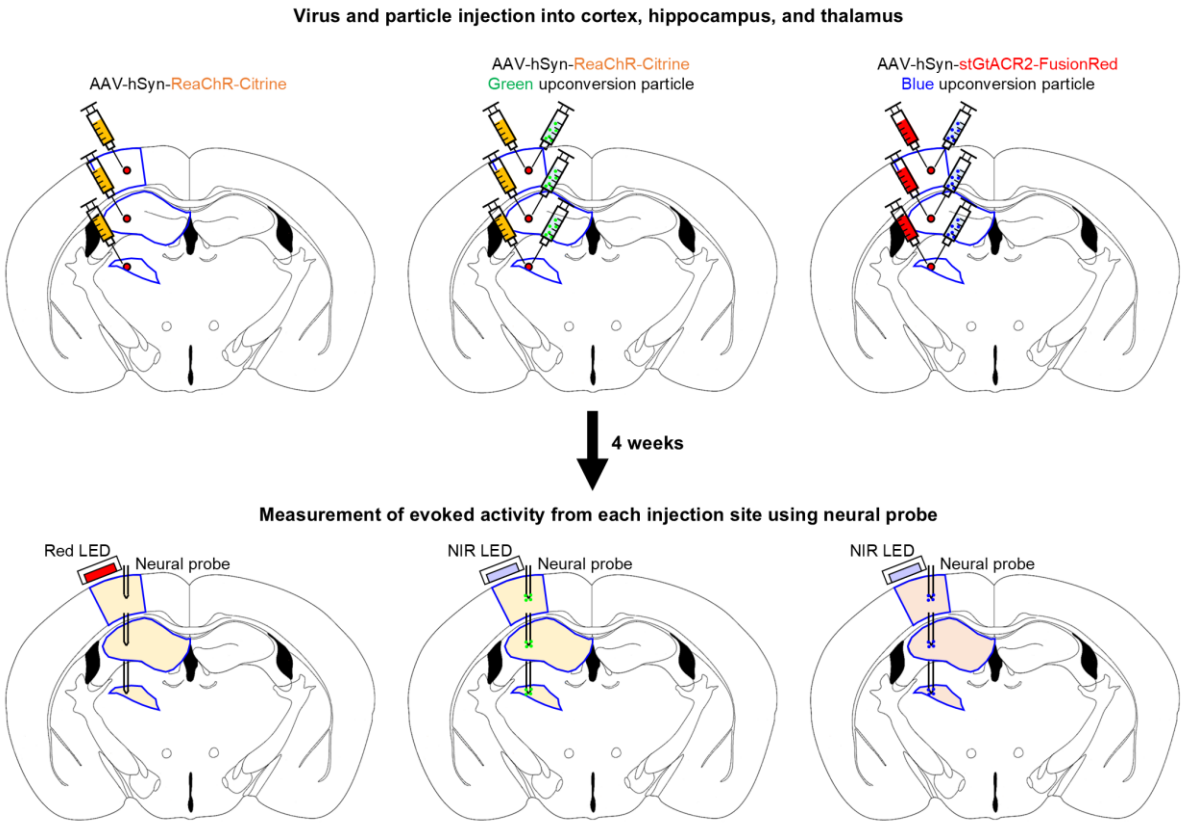

Supplementary Fig. 7: Schematic diagrams for virus/particle injection into various brain regions including cortex, hippocampus, and thalamus, for the electrophysiological experiment using the neural probe. The diagrams illustrate the depth of the injections and the location of the neural probe and the LEDs according to each combination.

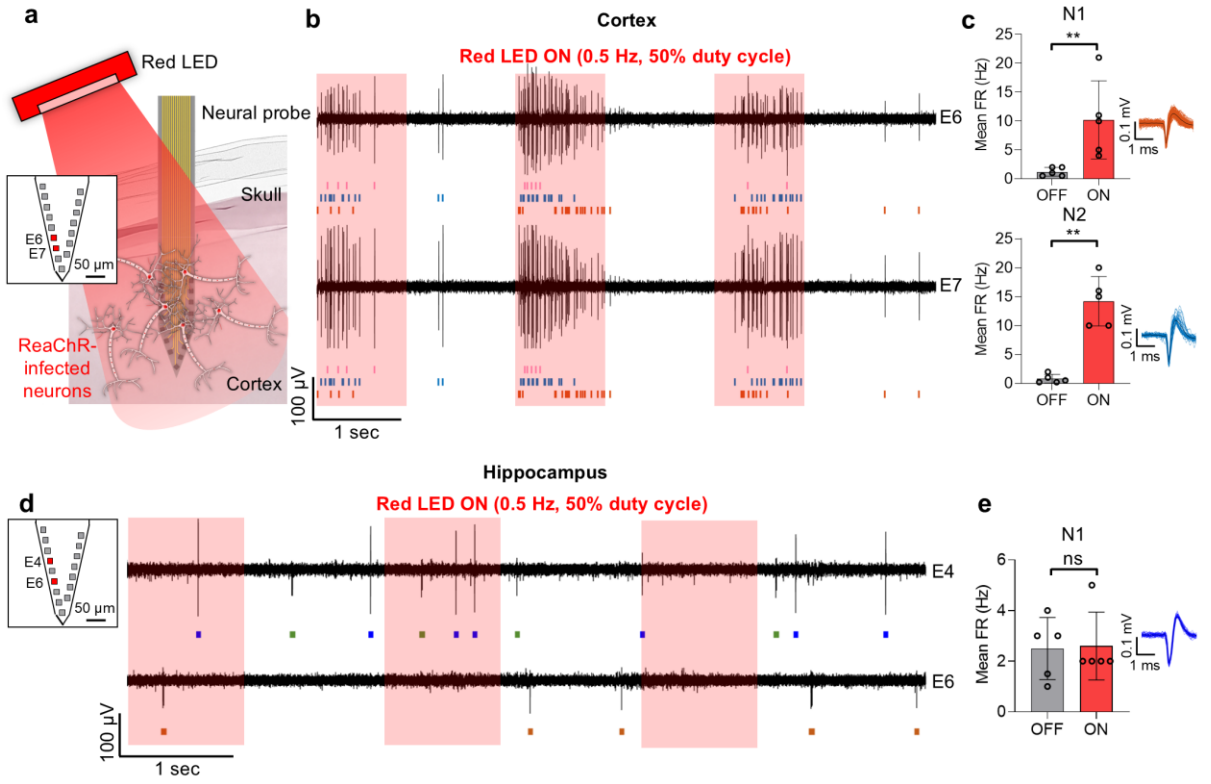

Supplementary Fig. 8: Transcranial optogenetic neuromodulation by red light in an anesthetized ReaChR-infected mouse. a Schematic diagram of optogenetic excitation by red light and neural signal recording using a neural probe in the sensory cortex region of the mouse. **b** Neural signals recorded from electrodes 6 and 7 in the sensory cortex region during light stimulation (0.5 Hz, 50% duty cycles; The red background indicates the onset of red LED). **c** Comparison of the firing rate recorded from neurons 1 and 2 between off and on cycles during light stimulation and sorted neural signals from the sensory cortex region (N1: p=0.0079; N2: p=0.0079, n=5 where n is the number of trials). **d** Neural signals recorded from electrodes 4 and 6 in the hippocampal CA3 region during light stimulation (0.5 Hz, 50% duty cycles; red background indicates the onset of red LED). **e** Comparison of the firing rate recorded from neuron 1 between off and on cycles during light stimulation and sorted neural signals from the hippocampal CA3 region (N1: p=0.9048, n=5 where n is the number of trials). The data are presented as mean values +/− s.d. Statistical analysis was performed by the two-tailed Mann-Whitney test, and p<0.05 was considered significant. ns: no statistical significance. ** p<0.01.

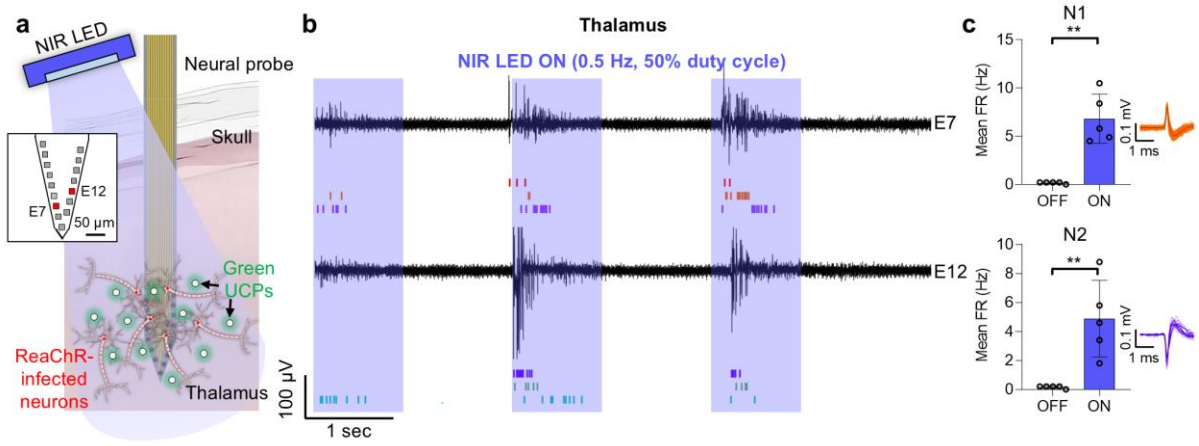

Supplementary Fig. 9: Transcranial optogenetic neuromodulation by NIR and Green UCPs in an anesthetized ReaChR-infected mouse. a Schematics of optogenetic excitation by NIR and green UCPs and neural signal recording using a neural probe in the thalamus region of the mouse. **b** Neural signals recorded from electrodes 7 and 12 in the thalamus region during light stimulation (0.5 Hz, 50% duty cycles; The blue background indicates the onset of NIR LED). **c** Comparison of the firing rate recorded from neurons 1 and 2 between off and on cycles during light stimulation and sorted neural signals (N1: p=0.0079; N2: p=0.0079, n=5 where n is the number of trials). The data are presented as mean values +/− s.d. Statistical analysis was performed by the two-tailed Mann-Whitney test, and $p<0.05$ was considered significant. ** $p<0.01$.

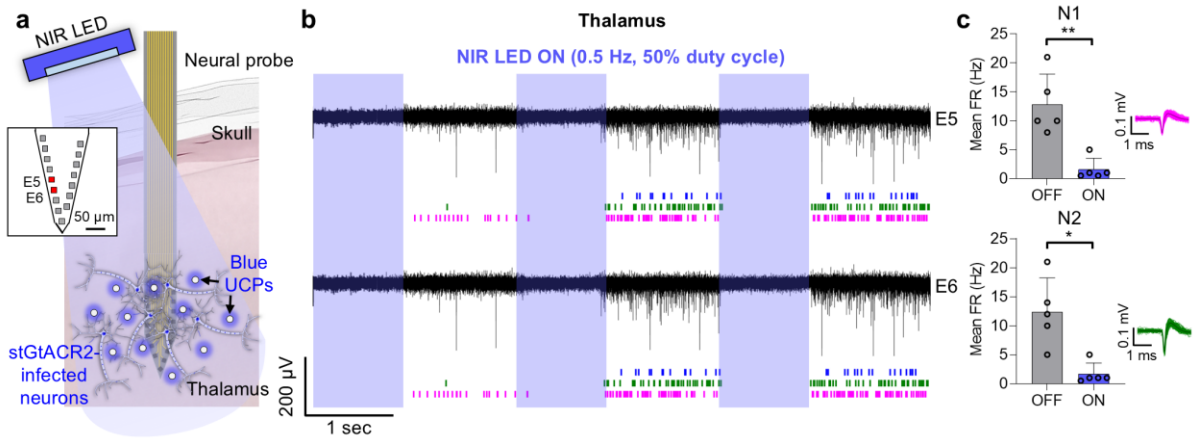

Supplementary Fig. 10: Transcranial optogenetic neuromodulation by NIR and Blue UCPs in an anesthetized stGtACR2-infected mouse. a Schematics of optogenetic inhibition by NIR and blue UCPs and neural signal recording using a neural probe in the thalamus region of the mouse. **b** Neural signals recorded from electrodes 5 and 6 in the thalamus region during light stimulation (0.5 Hz, 50% duty cycles; The blue background indicates the onset of NIR LED). **c** Comparison of the firing rate recorded from neurons 1 and 2 between off and on cycles during light stimulation and sorted neural signals (N1: p=0.0079; N2: p=0.0159, n=5 where n is the number of trials). The data are presented as mean values +/− s.d. Statistical analysis was performed by the two-tailed Mann-Whitney test, and $p<0.05$ was considered significant. * $p<0.05$, ** $p<0.01$.

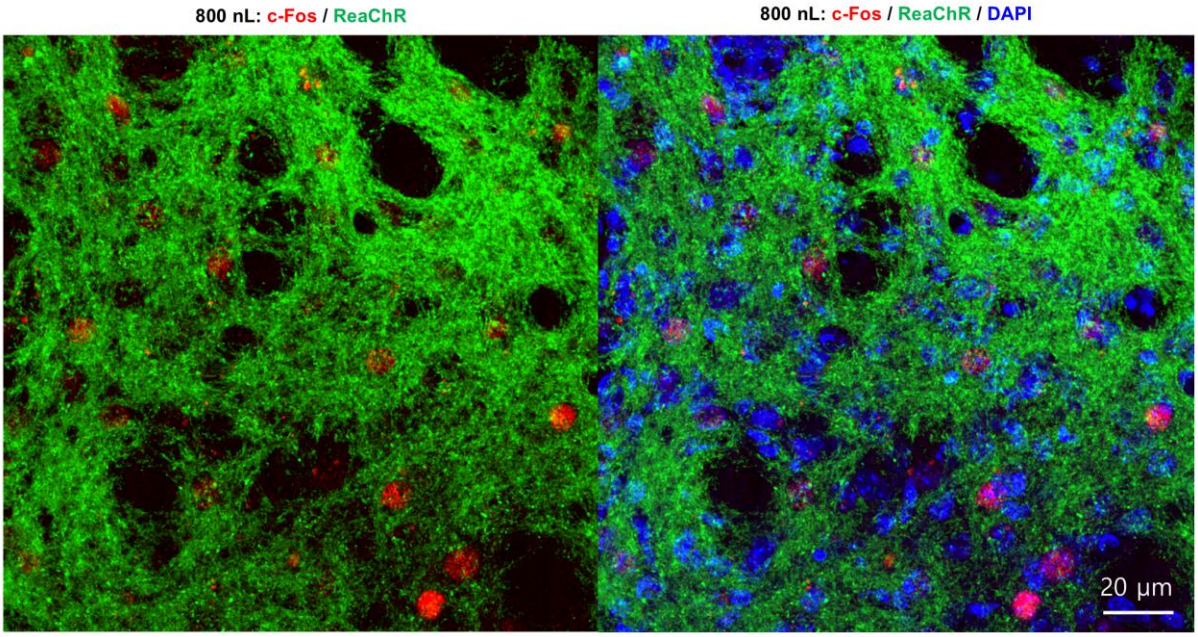

Supplementary Fig. 11: High-magnification representative confocal fluorescence images showing c-Fos expression induced by NIR stimulation in mice injected with virus and particles (800 nl). (Left) Image showing virus-infected neurons and c-Fos expression. (Right) Image showing virus-infected neurons, c-Fos expression, and DAPI staining. The c-Fos experiments were independently repeated in three mice with similar results to ensure reproducibility, and the representative images are shown in the figure.

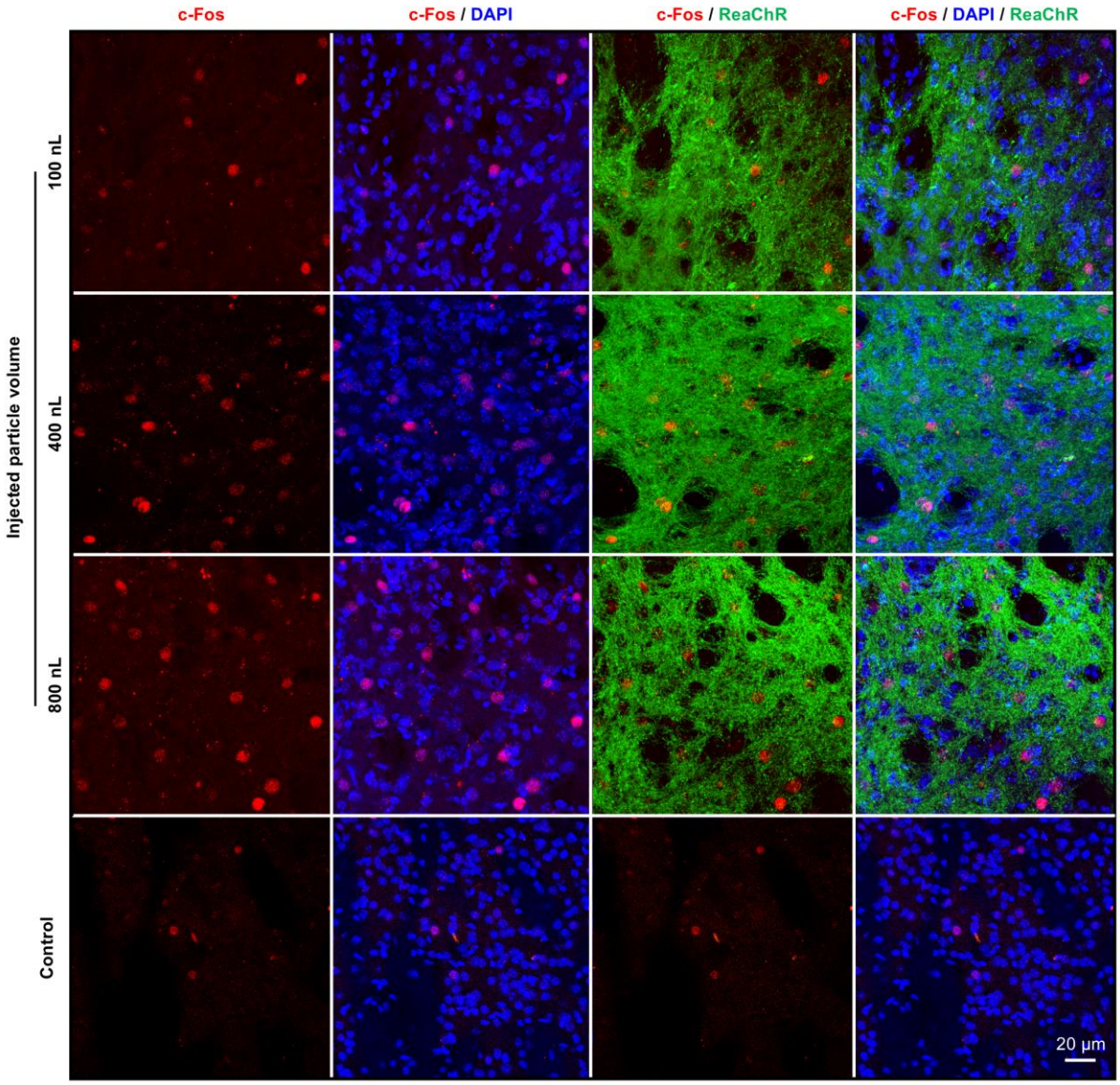

Supplementary Fig. 12: High-magnification fluorescence images showing c-Fos expression in the target region depending on the amount of particle injection. The control group represents mice that underwent NIR stimulation without the injection of both virus and particles. The c-Fos experiments were independently repeated in three mice with similar results to ensure reproducibility, and the representative images are shown in the figure.

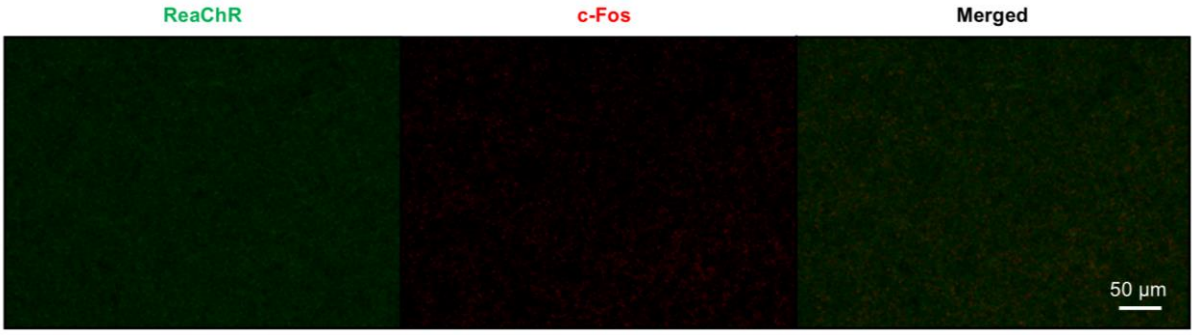

Supplementary Fig. 13: Representative confocal fluorescence image showing c-Fos expression induced by NIR stimulation in mice that were not injected with either virus or particles. The c-Fos experiments were independently repeated in three mice with similar results to ensure reproducibility, and the representative images are shown in the figure.

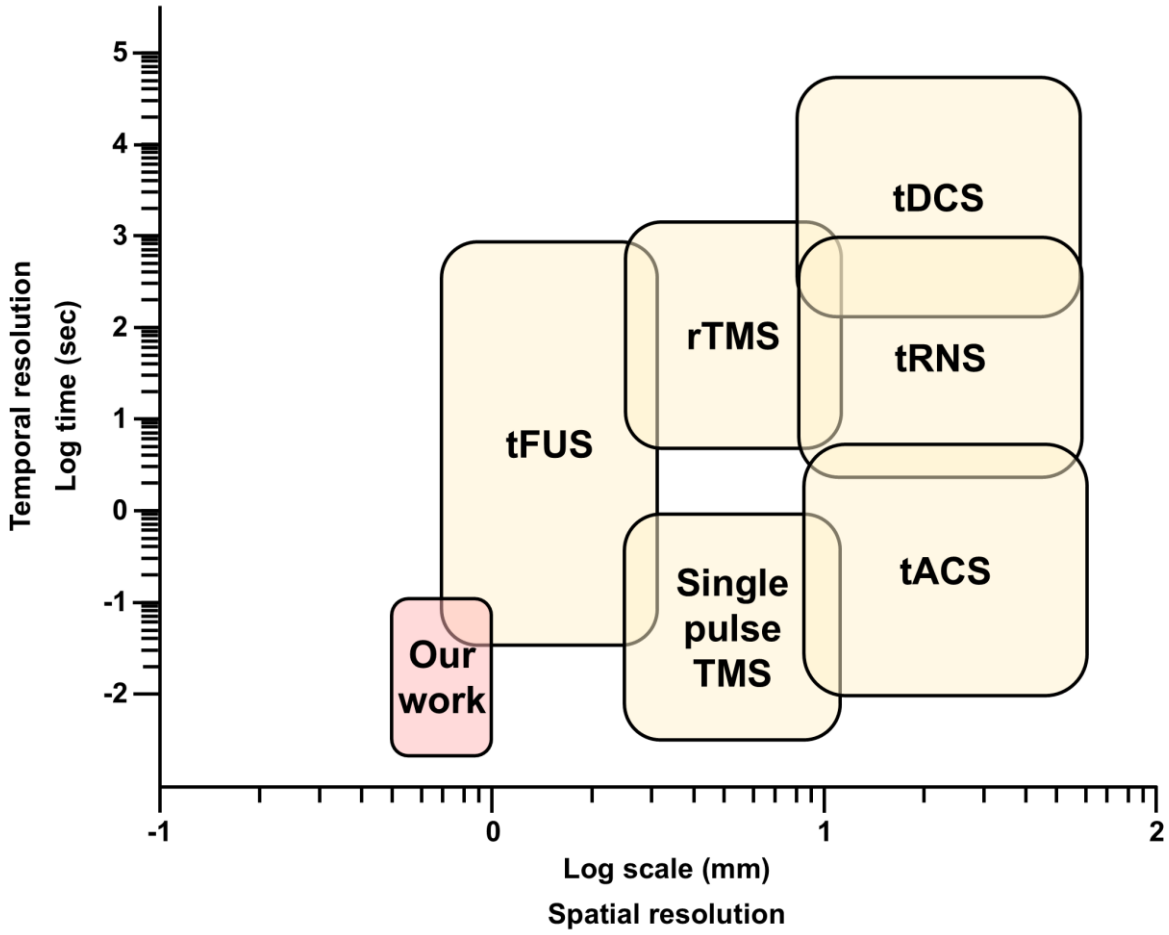

Supplementary Fig. 14: Comparison of temporal and spatial resolution in transcranial brain stimulation techniques[4,5]**.** Our work (pink shaded area) demonstrates higher spatial resolution (approximately 0.5 mm) compared to traditional non-invasive methods such as transcranial focused ultrasound stimulation (tFUS), repetitive transcranial magnetic stimulation (rTMS), transcranial direct current stimulation (tDCS), transcranial alternating current stimulation (tACS), transcranial random noise stimulation (tRNS), and single-pulse transcranial magnetic stimulation (single pulse TMS). The temporal and spatial resolutions are plotted on a logarithmic scale, highlighting the enhanced precision of our transcranial optogenetic neuromodulation approach for targeting specific brain regions effectively.

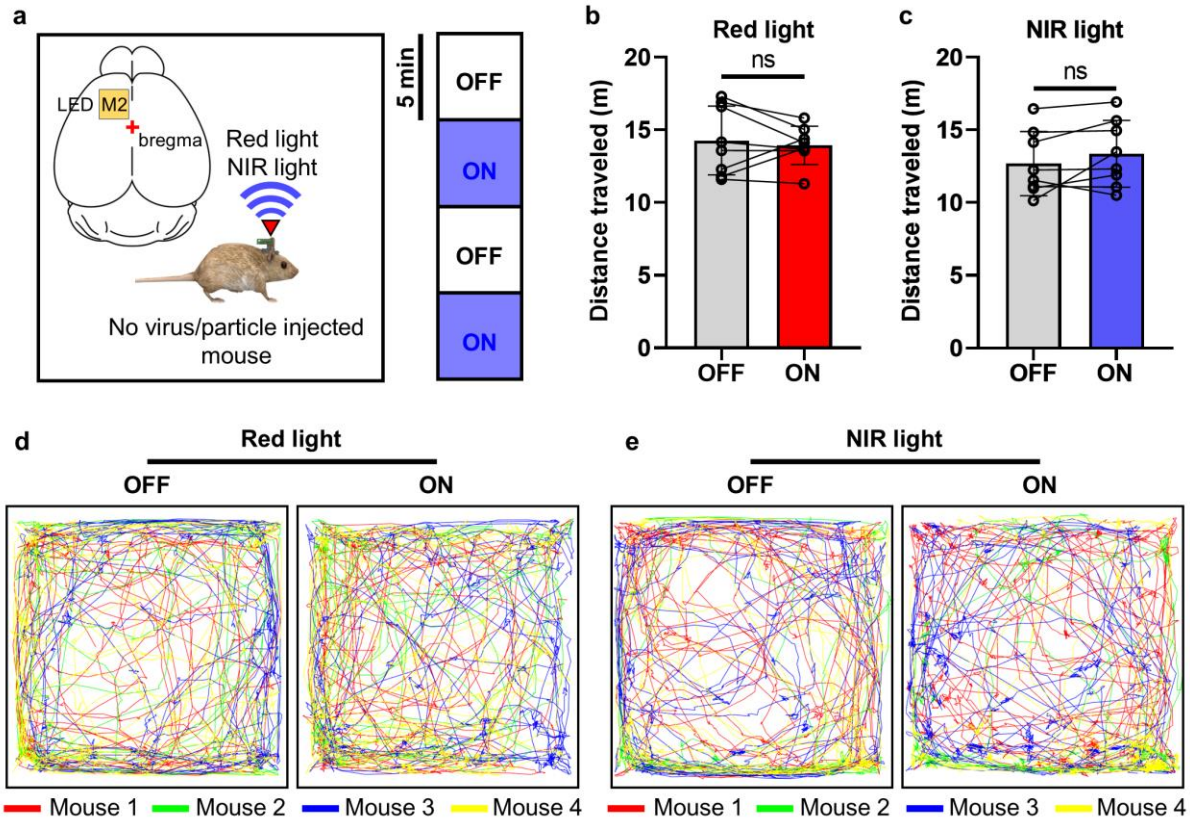

Supplementary Fig. 15: Effect of light delivery into the brain using the optoelectronic system on general locomotor activity. a Schematic illustration showing the experimental process. The inset displays the LED placement on the M2 region of the brain. Testing for light delivery consisted of two cycles. One cycle consisted of two 5 min epochs with alternating light delivery (OFF-ON). We operated the system with a 10 Hz frequency and a 10 ms ON time during stimulation. **b** Comparison of the distance traveled according to red LED on and off ($t(7)=0.5515$, $p=0.5985$). **c** Comparison of the distance traveled according to NIR LED on and off ($t(7)=1.459$, $p=0.1879$). **d** Trajectories of each mouse according to red LED on and off. The color of the line represents each mouse. **e** Trajectories of each mouse according to NIR LED on and off. The color of the line represents each mouse. The data are presented as mean values +/− s.d. with individual data points (white circle: n=8 for all data, n is the number of cycles. This experiment was conducted with four mice.). All statistical analyses were performed by the two-tailed Paired t test, and $p<0.05$ was considered significant. ns: no statistical significance.

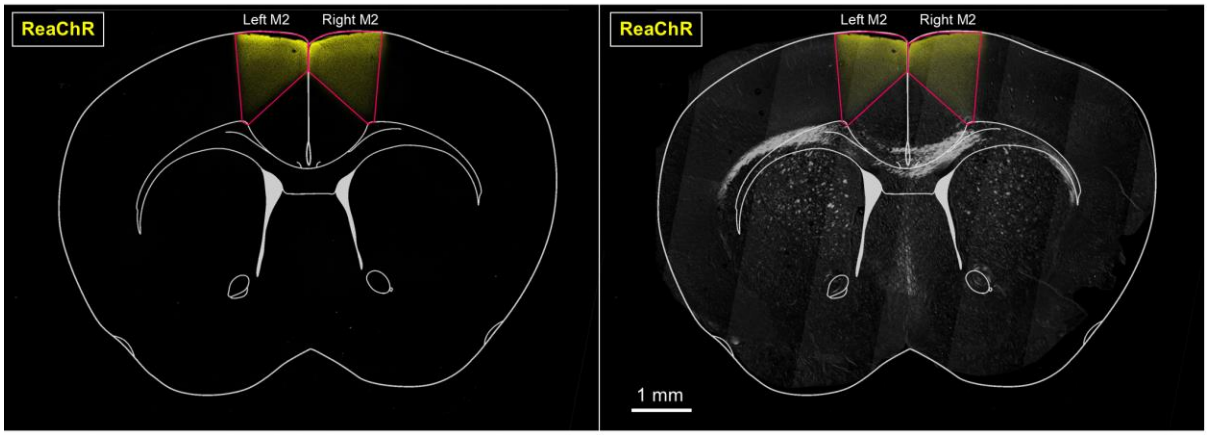

Supplementary Fig. 16: Representative confocal fluorescence images of ReaChR (Citrine) virus-infected neurons in the premotor cortex (M2) region. The left fluorescence image shows that only neurons in the M2 region are infected. The right fluorescence image was merged with a bright-field image. Virus expression was observed in at least three mice with similar results to ensure reproducibility, and representative images are shown in the figure.

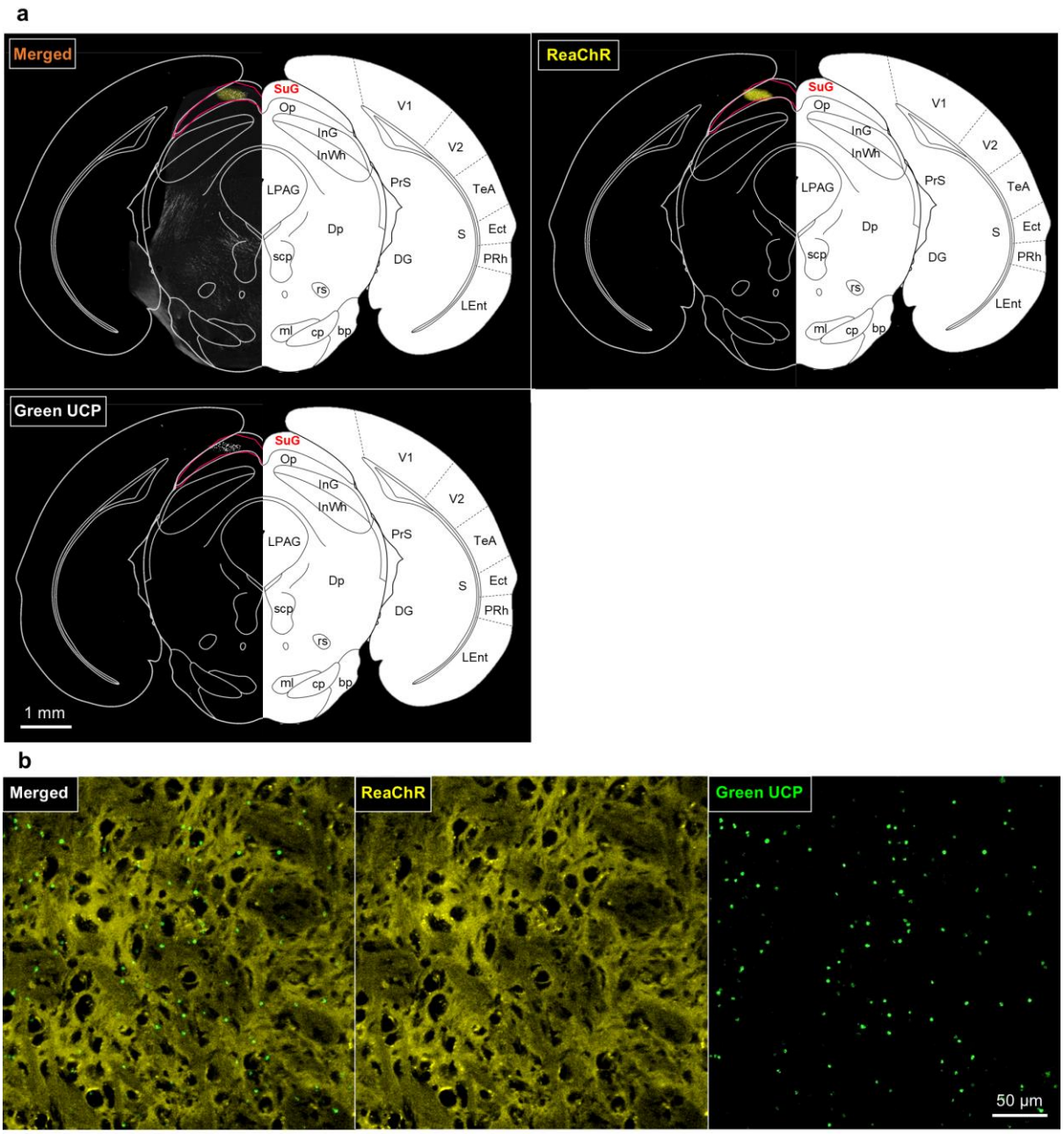

Supplementary Fig 17: Representative confocal fluorescence images of ReaChR (Citrine) virus-infected neurons and injected green upconversion particles (UCP) in superior colliculus (SC) region. a Fluorescence images that show infected neurons and injected particles in the SC region. **b** Expanded fluorescence images that show infected neurons and injected particles in the SC region. Virus expression and particle injection were observed in at least three mice with similar results to ensure reproducibility, and representative images are shown in the figure.

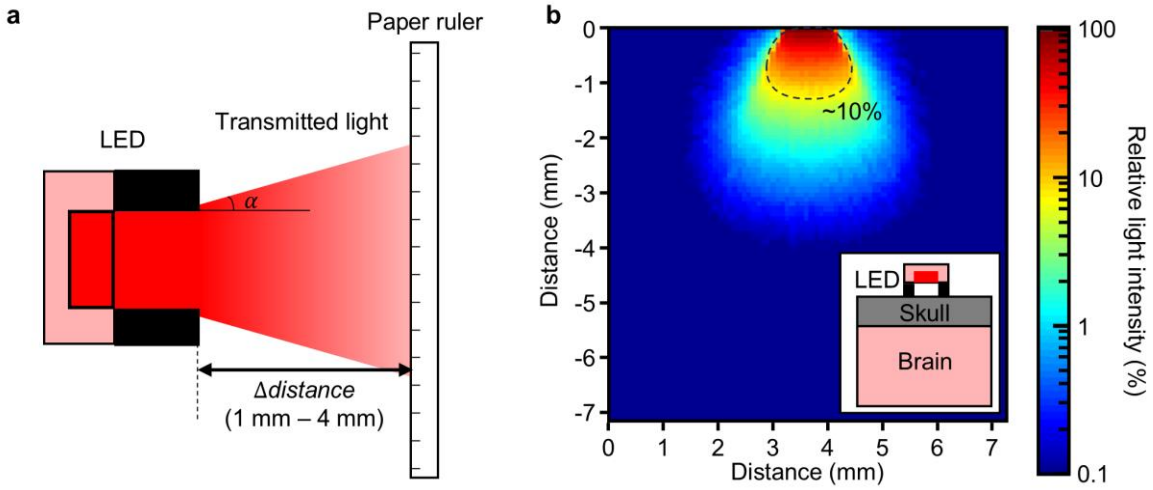

Supplementary Fig. 18: Light dispersion and simulation of LED operation. a Schematic representation of light dispersion measurement. The experimental setup used to measure the light dispersion angle (α) of the red LED. A paper ruler is positioned at varying distances (1 mm to 4 mm) from the LED to quantify the spread of transmitted light. The square piece is attached to the LED to limit the light spread. **b** Simulated light distribution within brain tissue. The Monte Carlo simulation results show the relative light intensity distribution within the brain, modeled to reflect in vivo conditions. The inset illustrates the position of the LED, skull, and brain.

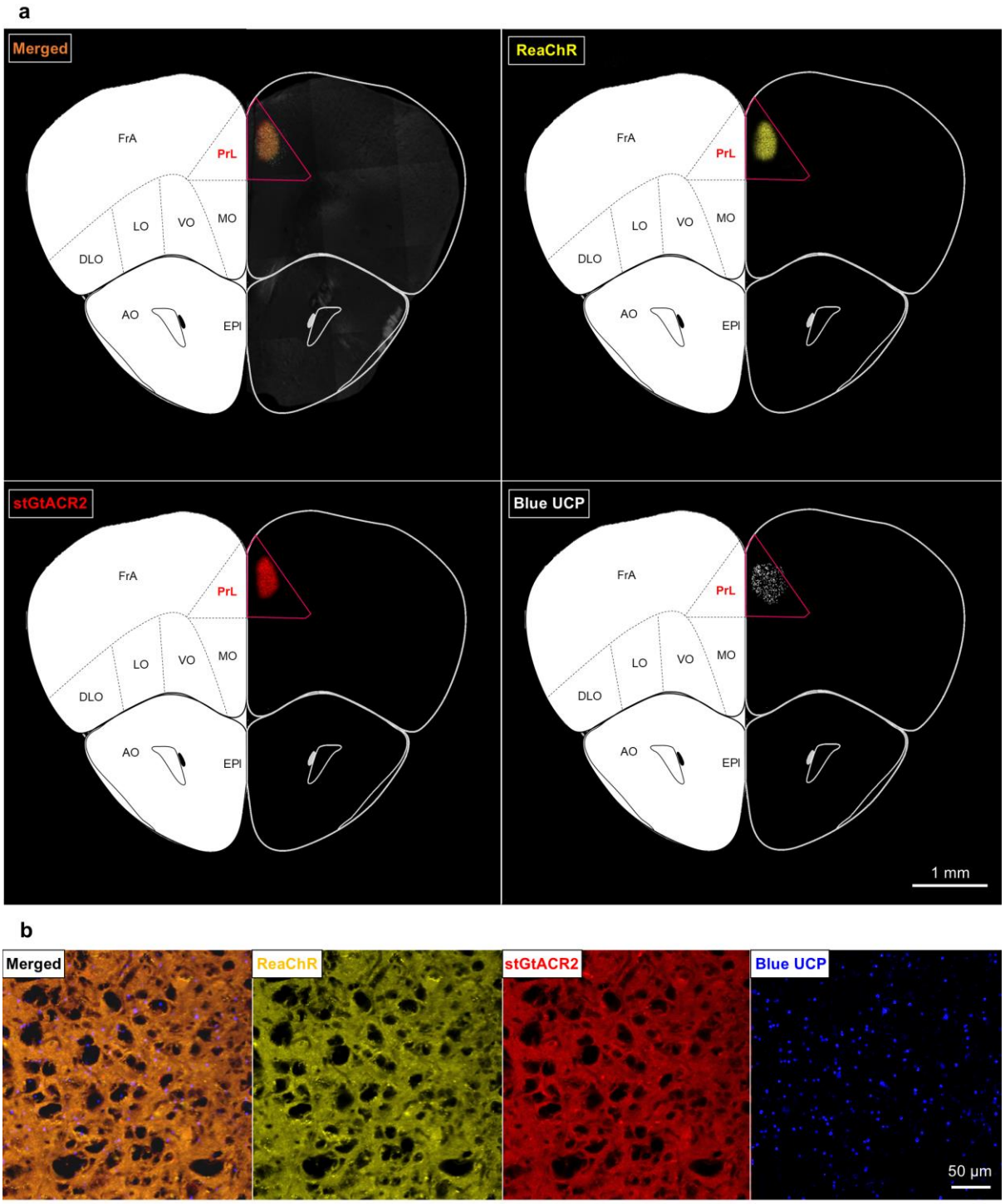

Supplementary Fig. 19: Representative confocal fluorescence images of ReaChR (Citrine) and stGtACR2 (FusionRed) viruses-infected neurons and injected blue upconversion particles (UCP) in medial prefrontal cortex (mPFC) region. a Fluorescence images that show infected neurons and injected particles in the mPFC region. **b** Expanded fluorescence images that show infected neurons and injected particles in the mPFC region. Virus expression and particle injection were observed in at least three mice with similar results to ensure reproducibility, and representative images are shown in the figure.

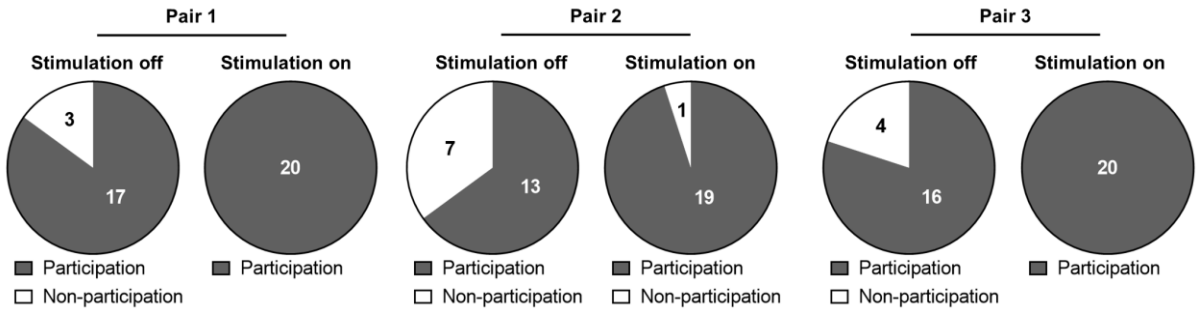

Supplementary Fig. 20: The number of participation or non-participation of each mouse pair according to stimulation off and on throughout food competition test (4 tests per pair). The two tests were conducted with stimulation on, and the other two tests were conducted with stimulation off.

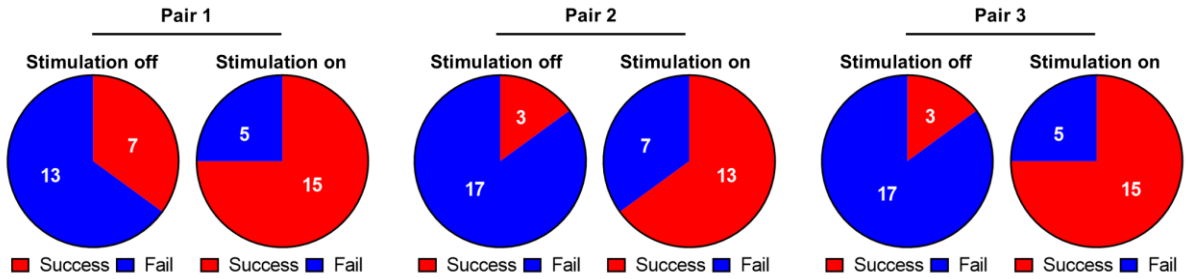

Supplementary Fig. 21: The number of successful extortion or failed extortion trials of each mouse pair according to stimulation on and off throughout the food competition test (4 tests per pair). Two tests were conducted with stimulation on, and the other two tests were conducted with stimulation off.

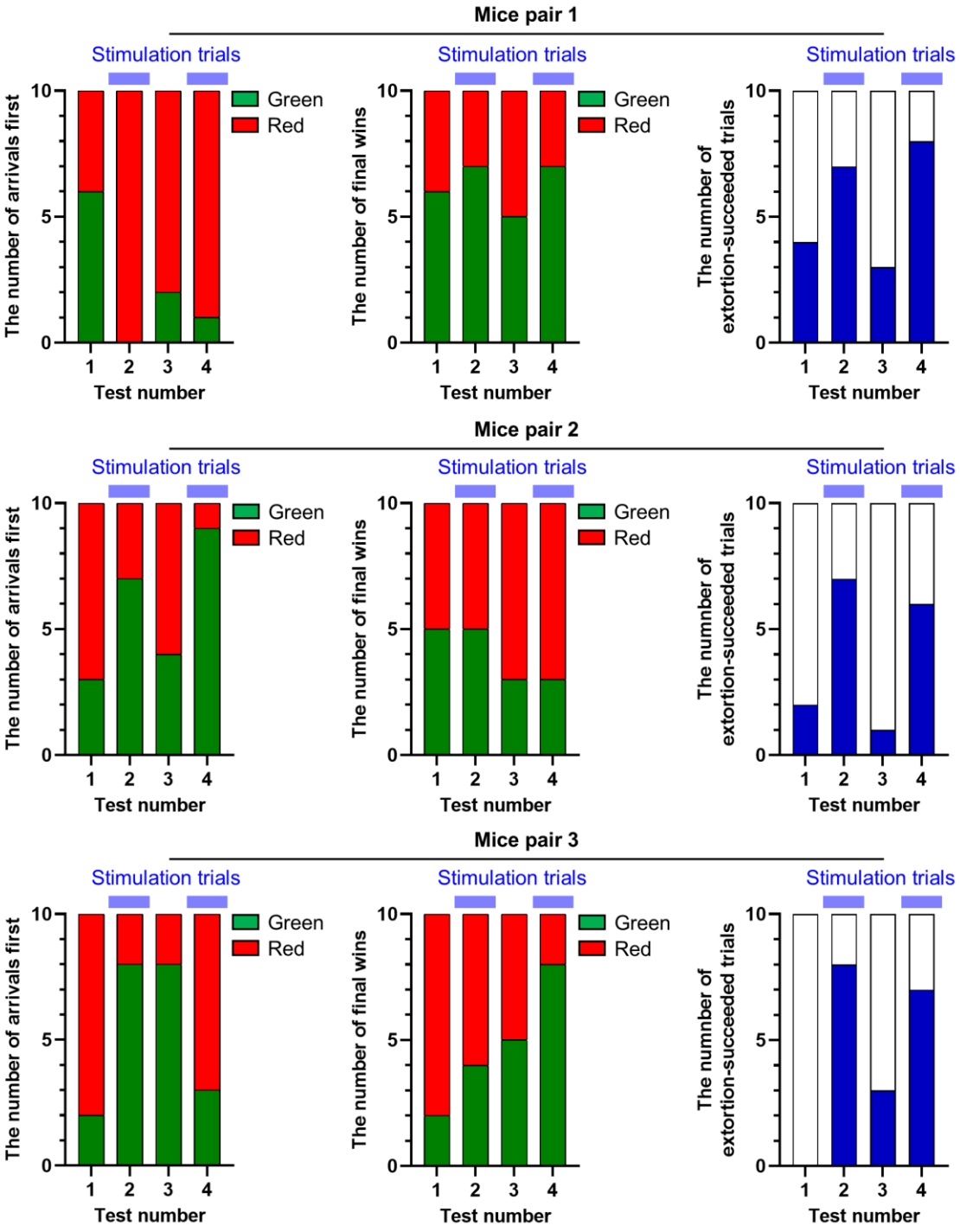

Supplementary Fig. 22: Detailed history of each mouse pair throughout the food competition test. Stacked bar plots show the number of arrivals, the number of final wins, and the number of extortion-succeeded trials according to stimulation off and on from each mouse pair.

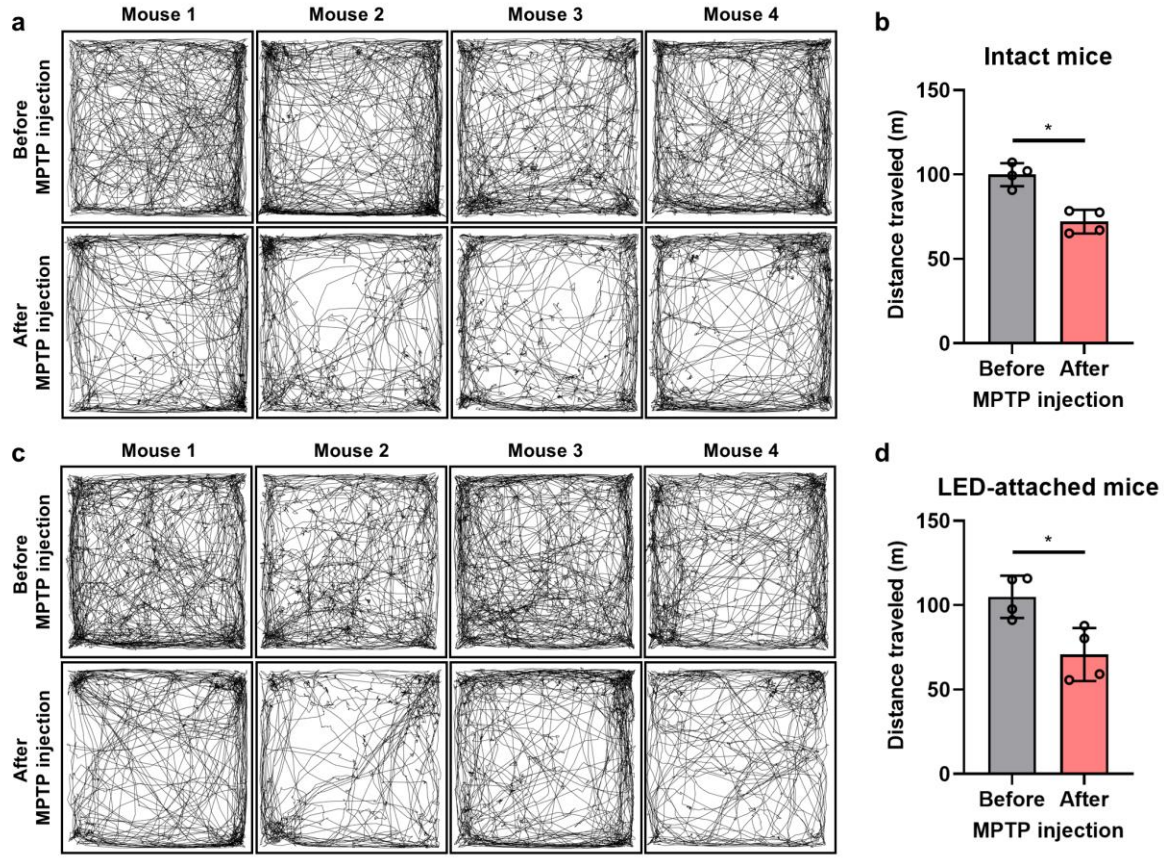

Supplementary Fig. 23: Effect of the MPTP injection on general locomotor activity. a Trajectories of each mouse before and after MPTP injection in intact mice for 30 min. **b** Comparison of the distance traveled before and after MPTP injection in intact mice ($p=0.0286$, white circle: $n=4$ where n is the number of mice.). **c** Trajectories of each mouse before and after MPTP injection in LED-attached mice for 30 min. **d** Comparison of the distance traveled before and after MPTP injection in LED-attached mice ($p=0.0286$, white circle: $n=4$ where n is the number of mice.). The data are presented as mean values +/− s.d. with individual data points. Statistical analysis was performed by the two-tailed Mann Whitney test, and $p<0.05$ was considered significant. * $p<0.05$.

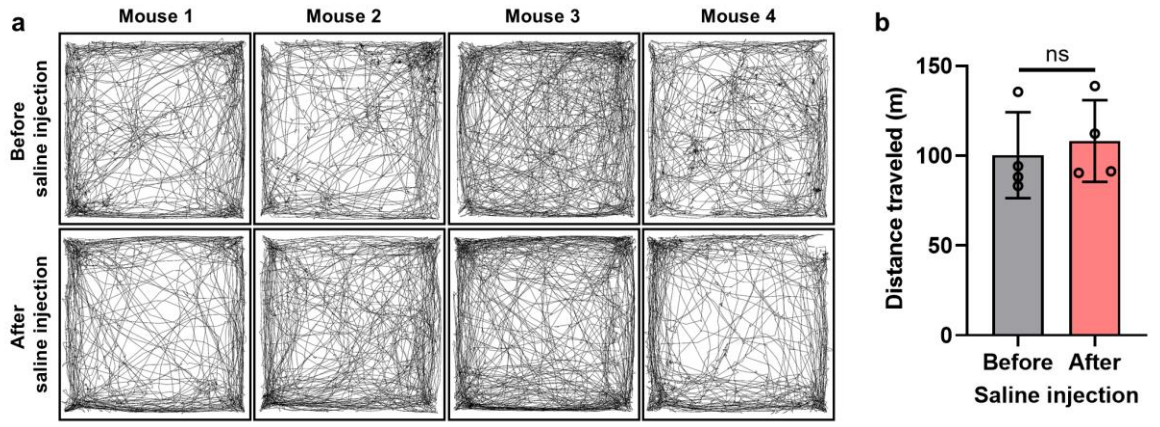

Supplementary Fig. 24: Effect of the saline injection on general locomotor activity. a Trajectories of each mouse before and after saline injection in intact mice for 30 min. **b** Comparison of the distance traveled before and after saline injection in intact mice ($p=0.4857$, white circle: $n=4$ where n is the number of mice.). The data are presented as mean values +/− s.d. with individual data points. Statistical analysis was performed by the two-tailed Mann-Whitney test. $p<0.05$ was considered significant. ns: no statistical significance.

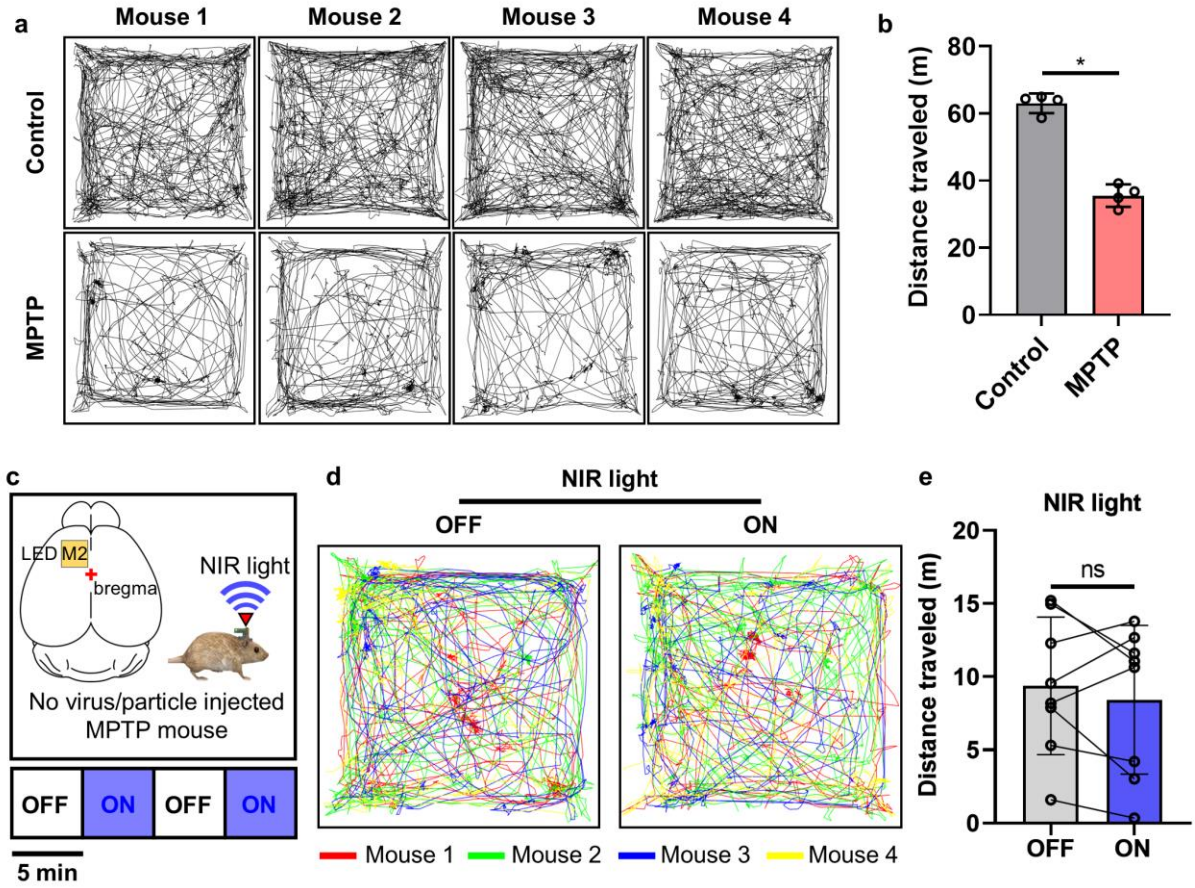

Supplementary Fig. 25: Effects of MPTP Injection and NIR Light on locomotor activity in mice. a Trajectories of each intact and MPTP-injected mouse for 20 min. **b** Comparison of the distance traveled for 20 min by intact and MPTP-injected mice ($p=0.0286$, white circle: $n=4$ where n is the number of mice.). **c** Schematic illustration showing the experimental process. The inset displays the LED placement on the M2 region of the brain. Testing for light delivery consisted of two cycles. One cycle consisted of two 5 min epochs with alternating light delivery (OFF-ON). We operated the system with a 10 Hz frequency and a 10 ms ON time during stimulation. **d** Trajectories of each mouse according to NIR LED on and off on the M2 region. The color of the line represents each mouse. **e** Comparison of the distance traveled according to red LED on and off on the M2 region ($p=0.4609$, white circle: $n=8$ for all data, where n is the number of cycles). The data are presented as mean values +/− s.d. with individual data points. Statistical analysis was performed by the two-tailed Mann-Whitney test (Supplementary Fig. 21b) and the Wilcoxon matched-pairs signed rank two-tailed test (Supplementary Fig. 21e). $p<0.05$ was considered significant. ns: no statistical significance.

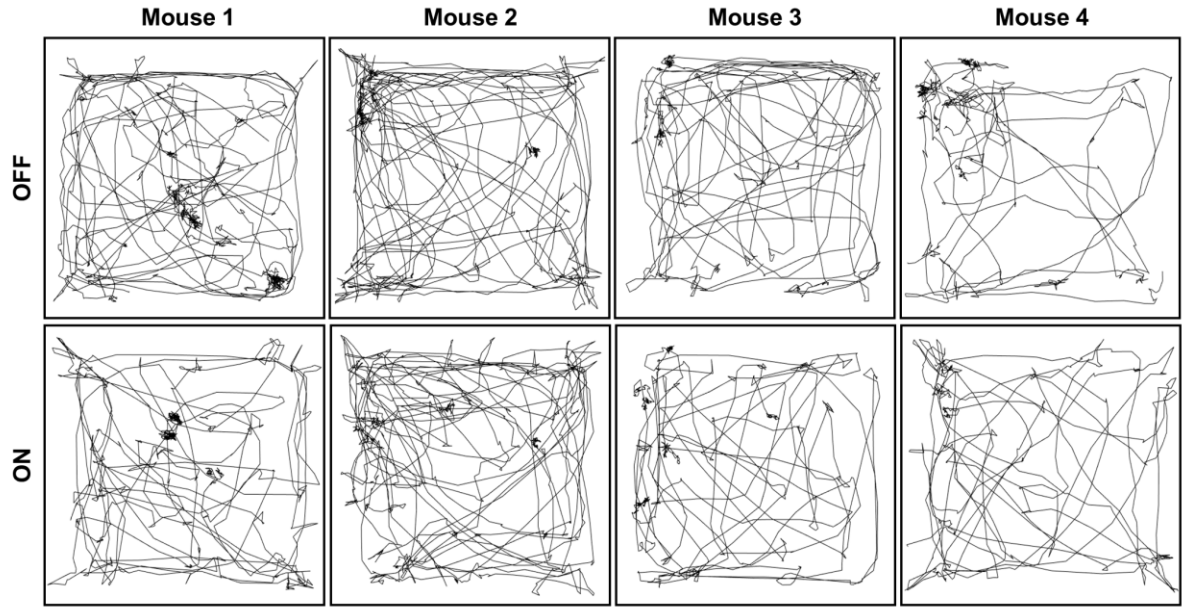

Supplementary Fig. 26: Movement trajectories of mice in open field tests with NIR stimulation. Trajectories of each mouse according to NIR LED on and off on the M2 region. We operated the system with a 10 Hz frequency and a 10 ms ON time during stimulation.

Supplementary Note 1. Estimation of the surface temperature of the brain caused by heat from the LED

To estimate the surface temperature of the brain caused by heat from the LED, we measured the temperature of the LED during operation.

The temperature difference (ΔT) across the skull can be calculated using:

$$\Delta T = \frac{d}{k} \times (T_{LED} - T_{brain})$$

In the equation, ΔT is the temperature difference, d is the skull thickness, and k is the thermal conductivity of the skull.

For example, if the LED temperature is 39.1°, we can estimate the surface temperature above the equation.

- Thermal conductivity of skull[6]: 0.32 W/m·K
- Skull thickness[7]: 0.25 mm
- LED temperature: 39.1°C

$$T_{brain} = T_{LED} - \Delta T = 39.1 - (39.1 - T_{brain}) \times \frac{0.00025}{0.32} = \frac{39.06945}{1.0008} \approx 39.04℃$$

This LED temperature can cause severe damage to the brain[8].

Supplementary Note 2. Calculation of the divergence angles for the light spread from the LED

To calculate the angle of divergence of the LED light source used in our experimental setup, we measured the light spread by placing a paper ruler at distances ranging from 1 mm to 4 mm from the LED. This setup allowed us to measure the diameter of the range of divergence at each distance.

The angle of divergence (α) was calculated using the tangent function:

$$\tan\left(\frac{\alpha}{2}\right) = \frac{\Delta W}{2\Delta D}$$

In the equation, ΔW is the change in the width of the light beam, ΔD is the change in distance.

For example, from 1 mm to 2 mm

- Width at 1mm (W_1): 2 mm
- Width at 2mm (W_2): 3 mm
- Distance Difference (ΔD): 2 mm – 1 mm = 1 mm
- Width Difference (ΔW): 3 mm – 2 mm = 1 mm

Using the equation:

$$\tan\left(\frac{\alpha}{2}\right) = \frac{1}{2 \times 1} = \frac{1}{2}$$

$$\alpha = 2 \times \arctan\left(\frac{1}{2}\right) \approx 2 \times 26.57° = 53.14°$$

Supplementary References

1 Li, L. *et al.* Colocalized, bidirectional optogenetic modulations in freely behaving mice with a wireless dual-color optoelectronic probe. *Nat Commun* **13**, 839, doi:10.1038/s41467-022-28539-7 (2022).

2 Kim, C. Y. *et al.* Soft subdermal implant capable of wireless battery charging and programmable controls for applications in optogenetics. *Nat Commun* **12**, 535, doi:10.1038/s41467-020-20803-y (2021).

3 Yang, Y. *et al.* Wireless multilateral devices for optogenetic studies of individual and social behaviors. *Nat Neurosci* **24**, 1035-1045, doi:10.1038/s41593-021-00849-x (2021).

4 Yang, D., Shin, Y. I. & Hong, K. S. Systemic Review on Transcranial Electrical Stimulation Parameters and EEG/fNIRS Features for Brain Diseases. *Front Neurosci* **15**, 629323, doi:10.3389/fnins.2021.629323 (2021).

5 Mosilhy, E. A. *et al.* Non-invasive transcranial brain modulation for neurological disorders treatment: A narrative review. *Life Sci* **307**, 120869, doi:10.1016/j.lfs.2022.120869 (2022).

6 Žák, J. *et al.* Model-based design of artificial zero power cochlear implant. *Mechatronics* **31**, 30-41, doi:10.1016/j.mechatronics.2015.04.018 (2015).

7 Ghanbari, L. *et al.* Craniobot: A computer numerical controlled robot for cranial microsurgeries. *Sci Rep* **9**, 1023, doi:10.1038/s41598-018-37073-w (2019).

8 Owen, S. F., Liu, M. H. & Kreitzer, A. C. Thermal constraints on in vivo optogenetic manipulations. *Nat Neurosci* **22**, 1061-1065, doi:10.1038/s41593-019-0422-3 (2019).